Research Article

STABLE CARBON ISOTOPE RECORD OF CARBONATE ACROSS THE CARNIAN–NORIAN BOUNDARY AT THE PROSPECTIVE GSSP SECTION AT BLACK BEAR RIDGE, BRITISH COLUMBIA, CANADA

Jerry Z. X. Lei[1], Jon M. Husson[1], Martyn L. Golding[2], Michael J. Orchard[2], and John-Paul Zonneveld[3]

[1]School of Earth and Ocean Sciences, University of Victoria, 3800 Finnerty Road, Bob Wright Centre A405. Victoria, British Columbia, Canada V8P 5C2. jerrylei@uvic.ca, jhusson@uvic.ca
[2]Geological Survey of Canada, Pacific - Vancouver, 605 Robson Street. Vancouver, British Columbia, Canada V6B 5J3. martyn.golding@canada.ca, mjorchard.micro@gmail.com
[3]Department of Earth and Atmospheric Sciences, University of Alberta, 1-26 Earth Sciences Building. Edmonton, Alberta, Canada T6G 2E3. zonnevel@ualberta.ca

Abstract – The Black Bear Ridge section is exposed on the shores of Williston Lake, British Columbia, Canada, with Late Triassic carbonate strata encapsulating the Carnian–Norian boundary as constrained by several fossil indices. Analysis of $\delta^{13}C_{carb}$ from this section reveals a six-meter-thick interval of increased instability proximal to the boundary. This excursion interval features anomalously low negative values, a shift of approximately -3 ‰ from the pre- and post- excursion interval values which average -0.95 ‰. It also features high point-to-point variability between these anomalously negative values and values comparable to the average outside of the excursion. This atypical feature of the excursion interval is interpreted to be the result of rapid, local-scale carbon cycle variation related to the global faunal turnover at the Carnian–Norian boundary, suggesting prolonged ecosystem instability around the stage boundary.

INTRODUCTION

The Black Bear Ridge section is exposed along the northern shore of Williston Lake. The continuous and abundantly fossiliferous limestone succession, which formed through deep marine deposition on the northwestern margin of Pangea, spans an interval stretching from the upper Carnian into the lower Hettangian (e.g., Zonneveld et al., 2010). This section is a strong candidate for the base-Norian Global Boundary Stratotype Section and Point (GSSP) (Orchard, 2007). The Carnian–Norian boundary interval (CNB) at Black Bear Ridge has been studied using a wide variety of approaches, including ammonoid biostratigraphy (Orchard et al., 2001; Balini et al., 2012), conodont biostratigraphy (Orchard, 2007, 2014, 2019), bivalve biostratigraphy (McRoberts, 2007, 2011), sedimentary facies (Zonneveld et al., 2010), $\delta^{13}C_{org}$ analysis (Williford et al., 2007a), $^{87}Sr/^{86}Sr$ chemostratigraphy (Onoue et al., 2016), and $\delta^{18}O_{PO4}$ chemostratigraphy (Sun et al., 2020). Ammonoids from Black Bear Ridge indicate the traditional CNB falls within an approximately six-meter interval that includes the first occurrance datum (FOD) of both the conodont *Metapolygnathus parvus* and the bivalve *Halobia austriaca* (Orchard, 2014). Both these species have been proposed as the defining fossil datum for the CNB (McRoberts & Krystyn, 2011; Mazza et al., 2018).

From prior studies, any $\delta^{13}C$ excursion at the CNB at Black Bear Ridge appears to be minor, with documented excursions inconsistent between studies. Williford et al. (2007a) found a small negative 0.5 ‰ excursion in $\delta^{13}C_{org}$ just above the base of the *Metapolygnathus parvus* Subzone. Subsequently, Onoue et al. (2016) conducted analysis of $\delta^{13}C_{carb}$ alongside other geochemical proxies across the CNB and found a positive shift of 1.5 ‰ in $\delta^{13}C_{carb}$ coinciding with the same datum. Major disturbances of global ocean $\delta^{13}C$ have been established to typically be preserved in both $\delta^{13}C_{carb}$ and $\delta^{13}C_{org}$ records, the assumption being the

Published online: March 12, 2021

Lei, J.Z.X., Husson, J.M., Golding, M.L., Orchard, M.J., & Zonneveld, J.-P. 2021. Stable carbon isotope record of carbonate across the Carnian–Norian boundary at the prospective GSSP section at Black Bear Ridge, British Columbia, Canada. *Albertiana*, vol. 46, 1–10.

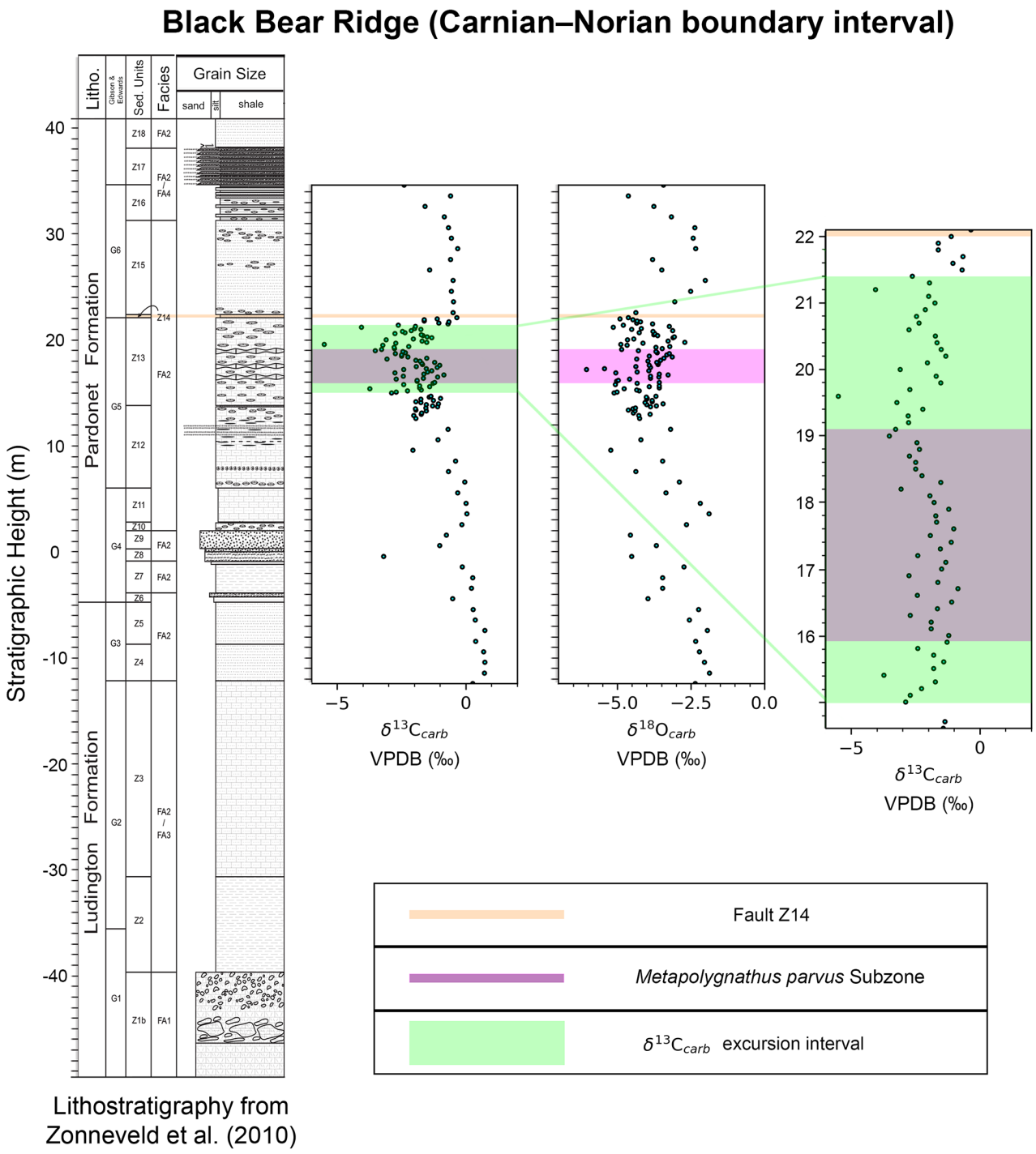

Figure 1–The CNB interval at Black Bear Ridge aligned with $\delta^{13}C_{carb}$, $\delta^{18}O_{carb}$, and zoomed-in $\delta^{13}C_{carb}$. A prominent excursion interval spanning 15.0–21.4 meters stratigraphically is highlighted in green. The *Metapolygnathus parvus* Subzone, as defined by the range of *M. parvus morphotype* alpha (Orchard, 2014), is highlighted in purple, spanning 15.9–19.1 meters stratigraphically. This representation is thicker than depicted in Orchard (2019, fig. 1), in order to more accurately reflect the thickness of the subzone as per Orchard (2019, figs. 2, 6). The 'Z14' fault is highlighted in orange.

organic material largely formed from the same dissolved inorganic carbon (DIC) pool (e.g., Kump & Arthur, 1999; Meyer el al., 2013). Strong correlations between the $\delta^{13}C_{carb}$ and $\delta^{13}C_{org}$ records are commonly utilized as evidence for primary signal preservation, since diagenesis would not alter the two records in parallel (e.g., Kump & Arthur, 1999; Meyer el al., 2013). This present study contributes a more complete high-resolution $\delta^{13}C_{carb}$ record for the CNB at Black Bear Ridge.

Beyond Black Bear Ridge, the $\delta^{13}C$ record for this stage boundary has been studied at a multitude of Tethyan sections, but with no greater consistency of signal. Muttoni et al. (2004) conducted $\delta^{13}C_{carb}$ analysis across the CNB boundary at Pizzo

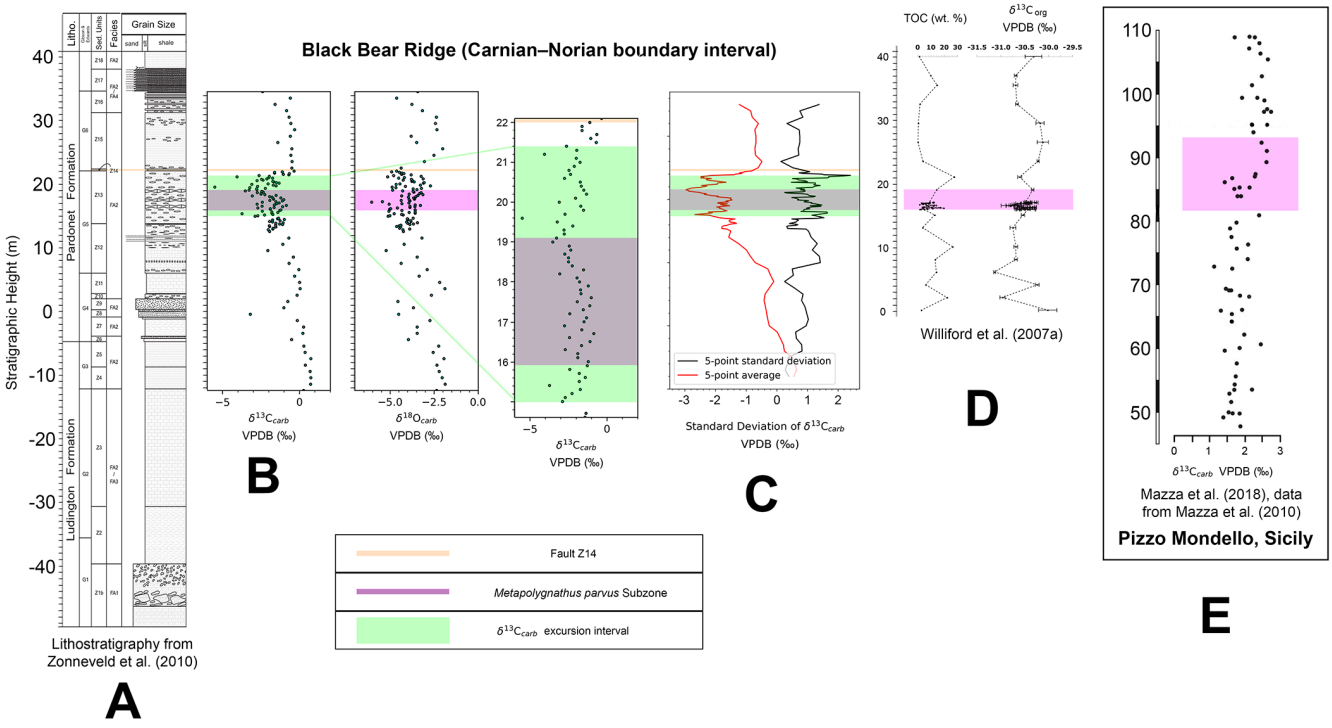

Figure 2 – Present study results aligned with select prior studies along the base of the *Metapolygnathus parvus* Subzone. All studies are displayed with the same scale for stratigraphic height except for the zoomed-in $\delta^{13}C_{carb}$ portion of the present study data. Also aligned is present study standard deviation and average $\delta^{13}C_{carb}$ calculated with a rolling set of five sequential data points.

Mondello, Italy, which is an alternate candidate for the base-Norian GSSP. A positive shift of 0.8 ‰ was identified just below the FOD of *Metapolygnathus parvus* (Muttoni et al., 2004, 2014). Mazza et al. (2010) also conducted $\delta^{13}C_{carb}$ analysis across the CNB at Pizzo Mondello and identified a positive shift of 0.6 ‰ at the same level, their T2 faunal turnover. Korte et al. (2005) conducted $\delta^{13}C_{carb}$ analysis across the CNB at Silická Brezová, Western Carpathians, but did not identify any excursions or shifts. Muttoni et al. (2014) conducted $\delta^{13}C_{carb}$ analysis across the CNB at Guri Zi, Albania, as well as at Aghia Marina, Greece. A minor positive shift of 0.3 ‰ was identified to coincide with the stage boundary in the former, whereas no shifts were identified in the latter. Jin et al. (2018, 2019) conducted $\delta^{13}C_{carb}$ and $\delta^{13}C_{org}$ analyses across the CNB at Hanwang, southern China, and identified a negative excursion of 4 ‰ and a positive shift of 2 ‰ respectively across the FOD of *M. parvus*. The negative excursion in $\delta^{13}C_{carb}$ is attributed to diagenesis, as only considering values from brachiopod shells displaying high preservation potential for primary $\delta^{13}C_{carb}$ signal reduces the excursion to a negative shift of 1 ‰ (Jin et al., 2018). Sun et al. (2019) conducted $\delta^{13}C_{carb}$ analysis at the Wadi Mayhah section in Oman and did not identify any excursions in the late Carnian through Norian portion of the section.

METHODS

Samples for $\delta^{13}C_{carb}$ were taken every meter throughout the Black Bear Ridge section, avoiding veins, soft-sediment deformation structures, bioclasts, and recrystallized zones when possible. Sampling density was increased to 10 cm for approximately 10 m through the CNB interval. Samples were cut into 1.2-cm-thick slabs, perpendicular to bedding when visible. The slabs were microdrilled using a carbide burr to extract approximately 60 mg of powder, preferentially from fine-grained calcite matrix and avoiding veins, bioclasts, and weathered surfaces. The powders were heated at 90°C for 12 hours to remove any moisture, then acidified with H_3PO_4 in airtight, helium flushed glass vials. $\delta^{13}C_{carb}$ and $\delta^{18}O_{carb}$ measurements were conducted at the University of Victoria on a Sercon 20-22 gas-source continuous-flow isotope ratio mass spectrometer with GasBox II front end. Measurements were corrected with internal standard VTS, and international standards IAEA-CO-8, and IAEA-603. Outliers were reanalyzed, measuring powder drilled from a different portion of the sample to ensure the results are not a product of measurement error nor intra-sample variability. Long-term standard reproducibility of the machine is calculated to be within 0.05–0.1 ‰ (1σ) for $\delta^{13}C_{carb}$, and within 0.15–0.2 ‰ (1σ) for $\delta^{18}O_{carb}$. Both $\delta^{13}C_{carb}$ and $\delta^{18}O_{carb}$ results are presented in delta notation relative to Vienna Pee Dee Belemnite (VPDB). Refer to Appendices 1 and 2 for tabulated measurements of all samples and standards.

RESULTS

$\delta^{13}C_{carb}$ values around the CNB at Black Bear Ridge largely fall between 1 and -2 ‰. A notable exception is an excursion interval

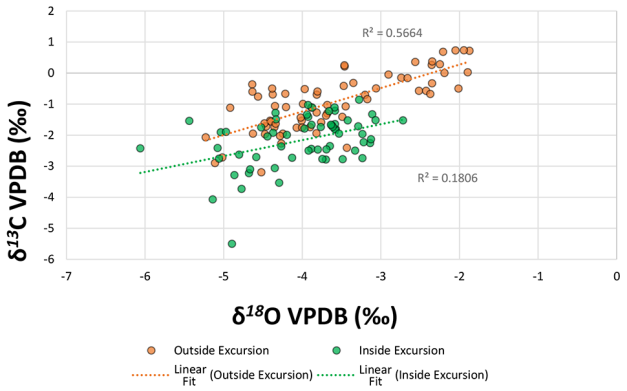

Figure 3–Correlation plot of $\delta^{13}C_{carb}$ vs. $\delta^{18}O_{carb}$ from the CNB at Black Bear Ridge, separating out data points within the excursion interval in green from data points outside the excursion interval in orange.

spanning 15.0–21.4 meters stratigraphically, where more negative values are observed and reach as low as -5.5 ‰, or -4.1 ‰ when excluding a $\delta^{13}C_{carb}$ single point outlier at 19.6 meters (Figure 1). Outside of this excursion interval, the average value for $\delta^{13}C_{carb}$ is -0.95 ‰. Single point outliers outside the excursion interval still reach low values, but no significant systematic shifts are observed, establishing a baseline range for typical $\delta^{13}C_{carb}$ values in the absence of major ecosystem disturbance. Inside of the excursion interval, the average value for $\delta^{13}C_{carb}$ is -2.2 ‰. However, 53% of $\delta^{13}C_{carb}$ values within the excursion interval still fall within the baseline range of 1 to -2 ‰, with the rest reaching lower values and resulting in high point-to-point variability. The excursion interval begins 0.9 meters below the base of the *Metapolygnathus parvus* Subzone and extends 2.3 meters above it (Figure 2A).

The excursion interval is defined by both the occurrence of $\delta^{13}C_{carb}$ values more negative than the background range observed further away from the CNB, as well as increased standard deviation. Standard deviation of $\delta^{13}C_{carb}$ is calculated with a rolling set of five sequential data points (the $\delta^{13}C_{carb}$ value at a given height, plus two above it, and two below it). A rolling 5-point average for $\delta^{13}C_{carb}$ is similarly calculated. These analyses show a series of standard deviation local maxima occur in the excursion interval, coinciding with a series of average $\delta^{13}C_{carb}$ local minima (Figure 2C). Increased standard deviation is also observed below the excursion interval at approximately 7–13 meters, however this does not coincide with average $\delta^{13}C_{carb}$ values as low as inside the excursion interval (Figure 2C). $\delta^{13}C_{carb}$ single point outliers at -0.4 and 19.6 meters are excluded in these analyses.

DISCUSSION

The $\delta^{13}C_{carb}$ values at the CNB of Black Bear Ridge are moderately well correlated with their corresponding $\delta^{18}O_{carb}$ values, indicating some degree of diagenetic influence on the $\delta^{13}C_{carb}$ record has likely occurred (Figure 3; Marshall, 1992). However, this correlation is much lower within the excursion interval at a R^2 value of 0.18, compared to the R^2 value of 0.57 outside. When excluding the $\delta^{13}C_{carb}$ single point outlier at 19.6 meters, the R^2 value within the excursion interval decreases further to 0.16. This suggests that while minor variations in $\delta^{13}C_{carb}$ values have likely been caused by diagenetic processes, the instability of the excursion interval shift could potentially be a primary, non-diagenetic signal.

Aligning the present study's results with the lithostratigraphy of Zonneveld et al. (2010), the excursion interval roughly correlates with sedimentary unit Z13, which lies entirely within the lithological facies FA2 of thin- / medium-bedded turbidites (Figure 2A). The lack of correlation with any lithological facies shift indicates that the $\delta^{13}C_{carb}$ signal is facies-independent, supporting primary seawater signal being preserved. Aligning the present study's results with the conodont biostratigraphy of Orchard (2019), the excursion is encompassed within the *Primatella primitia* Zone; it begins in the middle of the *Acuminatella acuminata-Parapetella prominens* Subzone, and extends through the *Metapolygnathus parvus* Subzone, into the lower portion of the *Primatella asymmetrica-Norigondolella* Subzone.

Comparing the Black Bear Ridge $\delta^{13}C_{org}$ results from Williford et al. (2007a) to the present study, the most extreme $\delta^{13}C_{carb}$ values observed in the present study excursion interval are beyond the portion that Williford et al. (2007a) sampled in 10 cm intervals (Figure 2D). Given the high point-to-point variability of the excursion interval, and how Williford et al. (2007a) increased the sampling interval to approximately 2–3 meters outside of this portion, it can be seen how Williford et al. (2007a) could have missed the excursion interval of the present study (Figure 2D).

Although several studies globally have proposed a positive shift in $\delta^{13}C$ at the CNB, issues such as small shift magnitude (Muttoni et al., 2004, 2014; Mazza et al., 2010), and poor sampling distribution (Onoue et al., 2016) makes the recognition of a positive shift questionable compared to background variation. Jin et al. (2019) provide a more convincing $\delta^{13}C_{org}$ positive shift in southern China, but this is not corroborated by $\delta^{13}C_{carb}$ results from the same section, which instead shows a negative excursion (Jin et al., 2018). The $\delta^{13}C_{carb}$ signal is dismissed as being caused by diagenesis because when utilizing only data points from select brachiopods, the negative excursion diminishes to a magnitude of approximately 1 ‰ (Jin et al., 2018). However, the positive shift in $\delta^{13}C_{org}$ of approximately 1.5 ‰ is not much larger than this brachiopod-carbonate negative excursion (Jin et al., 2018, 2019). Compounded by how $\delta^{13}C_{org}$ records tend to have higher amounts of variability than $\delta^{13}C_{carb}$ records (e.g., Kump & Arthur, 1999; Meyer el al., 2013), the $\delta^{13}C_{carb}$ negative excursion in southern China is no less convincing than the $\delta^{13}C_{org}$ positive shift (Jin et al., 2018, 2019). Compiling current results could suggest a global negative excursion in the $\delta^{13}C$ record at the CNB, but which is not preserved in western Tethyan sections (Muttoni et al., 2004, 2014; Korte et al., 2005; Williford et al., 2007a; Mazza et al., 2010; Onoue et al., 2016; Jin et al., 2018, 2019). However, the more likely alternative could be a lack of significant disturbance in the global $\delta^{13}C$ record at the CNB, with some manner of local effect creating the instability observed at Williston Lake and Hanwang (Muttoni et al., 2004, 2014; Korte et al., 2005; Williford et al., 2007a; Mazza et al., 2010; Onoue et al., 2016; Jin et al., 2018, 2019).

If the $\delta^{13}C_{carb}$ record preserves a perturbation to the global carbon cycle in the absence of local or diagenetic overprinting, the first-order expectation would be a systematic transition from excursion to post-excursion values (Kump & Arthur, 1999). An example would be the negative excursion in $\delta^{13}C$ established at the Triassic–Jurassic boundary, observed in many localities globally (e.g., Pálfy et al., 2007; Williford et al., 2007b). Many different mechanisms can potentially cause a negative excursion to be preserved in the $\delta^{13}C$ record. An example would include the collapse of marine productivity leading to less burial of organic matter, thus decreasing global ocean $\delta^{13}C$ (Kump, 1991). Alternatively, increasing global temperatures could dissociate sea floor methane clathrates, releasing large quantities of previously sequestered carbon with very negative $\delta^{13}C$ values, thus decreasing global ocean $\delta^{13}C$ (Dickens et al., 1995). The excursion interval observed at the CNB of Black Bear Ridge is of atypical pattern because of the rapid oscillation between anomalously negative values and values comparable to the -0.95 ‰ average outside of the excursion interval. A possible explanation is the local disruption of shallow marine carbonate formation in response to the global climatic change at the CNB. Geyman & Maloof (2019) describes a "diurnal carbon cycle engine" to explain modern Bahamian carbonate mud with positively shifted $\delta^{13}C$ precipitating in shallow marine environments, decoupled from global ocean values. During daytime, photosynthesis consumes dissolved CO_2, preferentially removing ^{12}C from the water and thus increasing $\delta^{13}C$ in the platform top environment. This $\delta^{13}C$ shift is countered by respiration at night. However, the decreased dissolved CO_2 during the day better facilitates carbonate precipitation, resulting in the carbonate recording heavier $\delta^{13}C$ values than global sea water (Geyman & Maloof, 2019). This effect would be expected most prominently in shallow waters that host extensive photosynthesis yet experience poor mixing (Geyman & Maloof, 2019). If the CNB is associated with a negative $\delta^{13}C_{carb}$ excursion in global seawater, intermittent positive shifts in $\delta^{13}C_{carb}$ stemming from local effects could result in the chaotically oscillating pattern (Figure 1). Alternatively, intermittent negative shifts in $\delta^{13}C_{carb}$ stemming from local effects could record a similar pattern in the absence of major disturbance in global sea water. Although Black Bear Ridge was not deposited in a restricted setting analogous to the Bahama Bank, carbonate sediment with these locally influenced shallow marine $\delta^{13}C_{carb}$ values could have been transported to deep marine settings by turbidity currents, for which there is abundant evidence at the CNB of Black Bear Ridge (Zonneveld et al., 2010). These periodic event beds would facilitate preservation of fine scale variations in the $\delta^{13}C_{carb}$ record originating from the shallow marine environment, which may differ from global ocean values (e.g., Patterson & Walter, 1994; Higgins et al., 2018). The length and chaotic nature of the excursion interval suggests prolonged environmental instability immediately prior and following the CNB. The $\delta^{18}O_{PO4}$ paleothermometry analysis of Sun et al. (2020) proposes an approximately 1.5-million-year period of rapid surface sea water temperature change, also suggesting prolonged environmental instability. The temperature rise within the CNB interval is immediately followed by a temperature fall (Sun et al., 2020). A subsequent pulse of temperature rise and fall extends the temperature perturbation interval well into the *Primatella asymmetrica-Norigondolella* Subzone (Sun et al., 2020).

Future complementary $\delta^{13}C_{org}$ analysis across the CNB at Black Bear Ridge could better determine to what extent the present study excursion interval is influenced by diagenesis. Continuous, well-preserved carbonate strata encompassing the CNB are exposed at a number of other sections in northeastern British Columbia. Future analysis at those sections similar to the present study could better define the geographic extent of this $\delta^{13}C$ excursion interval.

CONCLUSIONS

The CNB at Black Bear Ridge is associated with an interval of instability in the $\delta^{13}C_{carb}$ record around the *Metapolygnathus parvus* Subzone of the *Primatella primitia* Zone. This interval begins 0.9 meters below the base of the *M. parvus* Subzone within the *Acuminatella acuminata-Parapetella prominens* Subzone, and extends for 2.3 meters above it, into the *Primatella asymmetrica-Norigondolella* Subzone. This excursion interval displays high point-to-point variability, rapidly oscillating between anomalously low $\delta^{13}C_{carb}$ values and values comparable to the average outside of the excursion. This atypical feature is interpreted as the result of local carbon cycling being disrupted in response to the climatic perturbations at the CNB. The length of this excursion interval implies prolonged ecosystem instability around the stage boundary. Although the CNB can evidently be marked with significant disturbance in the $\delta^{13}C$ record, this proxy does not seem to occur with sufficiently global replicability for use as a universal marker (Muttoni et al., 2004, 2014; Korte et al., 2005; Williford et al., 2007a; Mazza et al., 2010; Onoue et al., 2016; Jin et al., 2018, 2019).

ACKNOWLEDGEMENTS

The authors would like to thank Morgan Weatherbie and Connor vanWieren for their hard work both in the field and in the lab. We also thank Travis Mayer and Alex Dyck of Williston Lake Outfitters for providing logistical support in the field. We also thank Mark Hounslow, Christopher McRoberts, and an anonymous reviewer for their helpful reviews and comments. This research was supported by a Natural Sciences and Engineering Research Council of Canada (NSERC) Discovery Grant to Jon Husson, and a NSERC Undergraduate Student Research Award to Morgan Weatherbie.

REFERENCES

Balini, M., Krystyn, L., Levera, M., & Tripodo, A. 2012. Late Carnian–Early Norian ammonoids from the GSSP candidate section Pizzo Mondello (Sicani Mountains, Sicily). Rivista Italiana di Paleontologia e Stratigrafia, 118: 47–84.

Dickens, G.R., Neil, J.R. O., Rea, D.K., & Owen, R.M. 1995. Dissociation of oceanic methane hydrate as a cause of the carbon isotope excursion at the end of the Paleocene.

Paleoceanography, 10(6): 965–971.

Geyman, E.C., & Maloof, A.C. 2019. A diurnal carbon engine explains 13C-enriched carbonates without increasing the global production of oxygen. Proceedings of the National Academy of Sciences of the United States of America, 116(49): 24433–24439.

Higgins, J.A., Blättler, C.L., Lundstrom, E.A., Santiago-Ramos, D.P., Akhtar, A.A., Crüger Ahm, A.S., Bialik, O., Holmden, C., Bradbury, H., Murray, S.T., & Swart, P.K. 2018. Mineralogy, early marine diagenesis, and the chemistry of shallow-water carbonate sediments. Geochimica et Cosmochimica Acta, 220: 512–534.

Jin, X., Shi, Z., Rigo, M., Franceschi, M., & Preto, N. 2018. Journal of Asian Earth Sciences Carbonate platform crisis in the Carnian (Late Triassic) of Hanwang (Sichuan Basin, South China): Insights from conodonts and stable isotope data. Journal of Asian Earth Sciences, 164: 104–124.

Jin, X., McRoberts, C.A., Shi, Z., Mietto, P., Rigo, M., Roghi, G., Manfrin, S., Franceschi, M., & Preto, N. 2019. The aftermath of the CPE and the Carnian–Norian transition in northwestern Sichuan basin, South China. Journal of the Geological Society, 176(1): 179–196.

Korte, C., Kozur, H.W., & Veizer, J. 2005. $\delta^{13}C$ and $\delta^{18}O$ values of Triassic brachiopods and carbonate rocks as proxies for coeval seawater and palaeotemperature. Palaeogeography, Palaeoclimatology, Palaeoecology, 226(3–4): 287–306.

Kump, L.R. 1991. Interpreting Carbon-Isotope Excursions: Strangelove Oceans. Geology, 19: 299–302.

Kump, L.R., & Arthur, M.A. 1999. Interpreting carbon-isotope excursions: Carbonates and organic matter. Chemical Geology, 161(1): 181–198.

Marshall, J.D. 1992. Climatic and oceanographic isotopic signals from the carbonate rock record and their preservation. Geological Magazine, 129(2): 143–160.

Mazza, M., Furin, S., Spötl, C., & Rigo, M. 2010. Generic turnovers of Carnian/Norian conodonts: Climatic control or competition? Palaeogeography, Palaeoclimatology, Palaeoecology, 290(1–4): 120–137.

Mazza, M., Nicora, A., & Rigo, M. 2018. *Metapolygnathus parvus* Kozur, 1972 (Conodonta): A potential primary marker for the Norian GSSP (Upper Triassic). Bollettino Della Societa Paleontologica Italiana, 57(2): 81–101.

McRoberts, C. A. 2007. The halobiid bivalve succession across a potential Carnian/Norian GSSP at Black Bear Ridge, Williston Lake, northeast British Columbia, Canada. Albertiana, 36: 142–145.

McRoberts, C.A. 2011. Late Triassic Bivalvia (chiefly Halobiidae and Monotidae) from the Pardonet Formation, Williston Lake area, northeastern British Columbia, Canada. Journal of Paleontology, 85(4): 613–664.

McRoberts, C.A., & Krystyn, L. 2011. The FOD of *Halobia austriaca* at Black Bear Ridge (northeastern British Columbia) as the base-Norian GSSP. 21st Canadian Paleontology Conference, UBC, August 19–21, Proceedings 9: 38–9.

Meyer, K.M., Yu, M., Lehrmann, D., van de Schootbrugge, B., & Payne, J.L. 2013. Constraints on Early Triassic carbon cycle dynamics from paired organic and inorganic carbon isotope records. Earth and Planetary Science Letters, 361: 429–435.

Muttoni, G., Kent, D.V., Olsen, P.E., Di Stefano, P., Lowrie, W., Bernasconi, S.M., & Hernández, F.M. 2004. Tethyan magnetostratigraphy from Pizzo Mondello (Sicily) and correlation to the Late Triassic Newark astrochronological polarity time scale. Bulletin of the Geological Society of America, 116(9–10): 1043–1058.

Muttoni, G., Mazza, M., Mosher, D., Katz, M.E., Kent, D. V., & Balini, M. 2014. A Middle–Late Triassic (Ladinian–Rhaetian) carbon and oxygen isotope record from the Tethyan Ocean. Palaeogeography, Palaeoclimatology, Palaeoecology, 399: 246–259.

Onoue, T., Zonneveld, J.-P., Orchard, M.J., Yamashita, M., Yamashita, K., Sato, H., & Kusaka, S. 2016. Paleoenvironmental changes across the Carnian/Norian boundary in the Black Bear Ridge section, British Columbia, Canada. Palaeogeography, Palaeoclimatology, Palaeoecology, 441: 721–733.

Orchard, M.J. 2007. A Proposed Carnian–Norian Boundary GSSP at Black Bear Ridge, northeast British Columbia, and a new conodont framework for the boundary interval. Albertiana, 36: 130–141.

Orchard, M.J. 2014. Conodonts from the Carnian–Norian Boundary (Upper Triassic) of Black Bear Ridge. New Mexico Museum of Natural History and Science Bulletin, 64, 146 pp.

Orchard, M.J. 2019. The Carnian–Norian boundary GSSP candidate at Black Bear Ridge, British Columbia, Canada: update, correlation, and conodont taxonomy. Albertiana, 45: 50–68.

Orchard, M.J., Zonneveld, J-P., Johns, M.J., McRoberts, C.A., Sandy, M.R., Tozer, E.T., & Carrelli, G.G. 2001. Fossil succession and sequence stratigraphy of the Upper Triassic and Black Bear Ridge, northeast B.C., and a GSSP prospect for the Carnian–Norian boundary. Albertiana, 25: 10–22.

Pálfy, J., Demény, A., Haas, J., Carter, E.S., Görög, Á., Halász, D., Oravecz-Scheffer, A., Hetényi, M., Márton, E., Orchard, M.J., Ozsvárt, P., Veto, I., & Zajzon, N. 2007. Triassic–Jurassic boundary events inferred from integrated stratigraphy of the Csovár section, Hungary. Palaeogeography, Palaeoclimatology, Palaeoecology, 244: 11–33.

Patterson, W.P., & Walter, L.M. 1994. Depletion of ^{13}C in seawater ΣCO_2 on modern carbonate platforms: significance for the carbon isotopic record of carbonates. Geology, 22(10): 885–888.

Sun, Y.D., Richoz, S., Krystyn, L., Zhang, Z.T., & Joachimski, M.M. 2019. Perturbations in the carbon cycle during the carnian humid episode: Carbonate carbon isotope records from southwestern China and Northern Oman. Journal of the Geological Society, 176(1): 167–177.

Sun, Y.D., Orchard, M.J., Kocsis, T., & Joachimski, M.M. 2020. Carnian–Norian (Late Triassic) climate change: Evidence from conodont oxygen isotope thermometry with implications for reef development and Wrangellian tectonics. Earth and Planetary Science Letters, 534: 116082.

Williford, K.H., Orchard, M.J., Zonneveld, J.-P., McRoberts, C.A., & Beatty, T.W. 2007a. A record of stable organic carbon isotopes from the Carnian–Norian boundary section at Black

Bear Ridge, Williston Lake, British Columbia. Albertiana, 36: 146–148.

Williford, K.H., Ward, P. D., Garrison, G. H., & Buick, R. 2007b. An extended organic carbon-isotope record across the Triassic–Jurassic boundary in the Queen Charlotte Islands, British Columbia, Canada. Palaeogeography, Palaeoclimatology, Palaeoecology, 244: 290–296.

Zonneveld, J.-P., Beatty, T.W., Williford, K.H., Orchard, M.J., & McRoberts, C.A. 2010. Stratigraphy and sedimentology of the lower Black Bear Ridge section, British Columbia: Candidate for the base-Norian GSSP. Stratigraphy, 7(1): 61–82.

APPENDIX 1—Measured $\delta^{13}C_{carb}$ and $\delta^{18}O_{carb}$ values for the Carnian–Norian boundary interval at the Black Bear Ridge section.

HEIGHT	$\delta^{13}C_{carb}$	$\delta^{18}O_{carb}$
-12.4	0.26	-2.35
-11.4	0.72	-1.87
-10.4	0.73	-2.05
-9.4	0.69	-2.21
-8.4	0.37	-2.35
-7.4	0.74	-1.94
-6.4	0.36	-2.56
-5.4	0.28	-2.25
-4.4	-0.51	-3.97
-3.4	0.21	-3.46
-2.4	0.25	-3.46
-1.4	-0.15	-2.74
-0.4	-3.19	-4.52
-0.4 RERUN	-2.74	-4.85
0.6	-1.03	-3.68
1.6	-0.76	-4.56
2.6	-0.16	-2.66
3.6	0.03	-1.89
4.6	0.00	-2.19
5.6	-0.32	-3.35
6.6	-0.05	-2.90
7.6	-0.69	-4.38
8.6	-0.41	-3.47
9.6	-2.07	-5.23
10.6	-1.09	-4.21
11.6	-0.70	-3.20
12.6	-1.95	-4.25
12.9	-2.03	-4.28
13	-1.74	-3.90
13.1	-1.72	-4.46
13.3	-1.53	-4.41
13.4	-1.95	-4.63
13.5	-1.97	-4.47
13.6	-1.56	-4.40
13.7	-1.11	-3.89
13.8	-1.29	-3.68
13.9	-1.54	-4.01
14	-1.07	-3.45
14.1	-1.76	-4.07
14.2	-1.94	-3.82
14.3	-1.27	-3.82
14.4	-1.75	-4.00
14.5	-1.00	-3.99
14.6	-1.43	-4.02
14.7	-1.37	-3.70
15	-2.90	-5.11
15.1	-2.72	-5.02
15.2	-2.27	-4.27
15.3	-1.74	-4.35
15.4	-3.73	-4.77
15.5	-1.80	-3.57
15.6	-1.41	-3.92
15.7	-1.81	-3.58
15.8	-2.41	-5.08
15.9	-1.28	-4.34
16	-1.21	-3.58
16.1	-1.91	-5.04
16.2	-1.89	-4.97
16.3	-2.70	-4.59
16.4	-1.66	-3.88
16.5	-1.11	-3.59
16.6	-2.44	-3.88
16.7	-0.86	-3.28
16.8	-1.64	-3.58
16.9	-2.76	-5.06
17	-1.49	-4.33

APPENDIX 1 (Continued)

HEIGHT	$\delta^{13}C_{carb}$	$\delta^{18}O_{carb}$
17.1	-1.34	-3.94
17.2	-2.42	-6.06
17.3	-1.54	-5.44
17.4	-1.11	-3.87
17.5	-1.92	-4.37
17.6	-1.03	-3.93
17.7	-1.68	-3.62
17.8	-1.73	-3.61
17.9	-1.22	-3.66
18	-1.79	-3.97
18.1	-1.95	-3.53
18.2	-3.06	-4.35
18.3	-1.52	-3.42
18.4	-2.25	-3.14
18.5	-2.50	-3.92
18.6	-2.50	-3.33
18.7	-2.74	-3.23
18.8	-2.35	-3.65
18.9	-2.46	-3.69
19	-3.53	-4.29
19.1	-3.29	-4.86
19.2	-2.77	-3.49
19.3	-2.79	-3.70
19.4	-2.23	-3.22
19.5	-3.23	-4.68
19.6	-5.50	-4.89
19.6 RERUN	-5.39	-4.58
19.7	-2.73	-4.13
19.8	-1.52	-2.72
19.9	-1.71	-3.29
20	-3.10	-4.66
20.1	-2.04	-4.44
20.2	-1.32	-3.11
20.3	-1.52	-3.07
20.4	-1.67	-3.63
20.5	-1.74	-3.76
20.6	-2.76	-3.74
20.7	-2.36	-4.27
20.8	-2.46	-3.80
20.9	-2.13	-3.12
21	-1.75	-4.52
21.1	-1.99	-4.20
21.2	-4.07	-5.14
21.3	-1.96	-3.23
21.4	-2.63	-4.80
21.5	-0.69	-3.81
21.6	-1.06	-4.35
21.7	-0.67	-4.22
21.8	-1.63	-4.34
21.9	-1.62	-4.48
22	-1.12	-4.92
22.1	-0.36	-4.64
22.6	-0.50	-4.38
23.6	-0.49	-3.06
24.6	-0.57	-2.52
25.6	-0.50	-2.01
26.6	-1.41	-3.49
27.6	-0.59	-3.81
28.6	-0.33	-2.35
29.6	-0.57	-2.42
30.6	-0.67	-2.37
31.6	-0.84	-3.17
32.6	-1.58	-3.76
33.6	-0.60	-4.63
34.6	-2.41	-3.43

APPENDIX 2—Analytical standard analyses for $\delta^{13}C_{carb}$ and $\delta^{18}O_{carb}$.

STANDARD	$\delta^{13}C_{carb}$	$\delta^{18}O_{carb}$
VTS	-1.65	-8.49
VTS	-1.53	-8.60
VTS	-1.51	-8.51
VTS	-1.54	-8.66
VTS	-1.49	-8.93
VTS	-1.46	-8.61
VTS	-1.47	-8.75
VTS	-1.56	-8.79
VTS	-1.54	-8.78
VTS	-1.24	-8.10
VTS	-1.26	-8.15
VTS	-1.55	-8.58
VTS	-1.40	-8.56
VTS	-1.43	-8.47
VTS	-1.54	-8.72
VTS	-1.51	-8.76
VTS	-1.52	-8.72
VTS	-1.49	-8.70
VTS	-1.53	-8.73
VTS	-1.53	-8.76
VTS	-1.63	-8.71
VTS	-1.62	-8.66
VTS	-1.59	-8.35
VTS	-1.54	-8.59
VTS	-1.47	-8.68
VTS	-1.49	-8.93
VTS	-1.59	-8.66
VTS	-1.52	-8.59
VTS	-1.54	-8.64
VTS	-1.48	-8.57
VTS	-1.46	-8.68
VTS	-1.40	-8.77
VTS	-1.55	-8.48
VTS	-1.55	-8.76
VTS	-1.39	-8.04
VTS	-1.67	-8.35
VTS	-1.55	-8.56
VTS	-1.43	-8.74
VTS	-1.53	-8.72
VTS	-1.60	-8.60
VTS	-1.49	-8.67

STANDARD	$\delta^{13}C_{carb}$	$\delta^{18}O_{carb}$
VTS	-1.42	-8.66
VTS	-1.45	-8.74
VTS	-1.45	-8.53
VTS	-1.54	-8.56
VTS	-1.57	-8.55
VTS	-1.48	-8.66
VTS	-1.54	-8.69
IAEA-CO-8	-5.78	-22.80
IAEA-CO-8	-5.77	-22.82
IAEA-CO-8	-5.70	-22.55
IAEA-CO-8	-5.73	-22.95
IAEA-CO-8	-5.68	-22.73
IAEA-CO-8	-5.72	-22.84
IAEA-CO-8	-5.68	-23.03
IAEA-CO-8	-5.80	-22.83
IAEA-CO-8	-5.52	-22.53
IAEA-CO-8	-5.64	-22.91
IAEA-CO-8	-5.68	-22.81
IAEA-CO-8	-5.69	-22.96
IAEA-CO-8	-5.72	-22.90
IAEA-CO-8	-5.71	-23.03
IAEA-CO-8	-5.72	-23.08
IAEA-CO-8	-5.75	-23.01
IAEA-CO-8	-5.75	-22.66
IAEA-CO-8	-5.79	-22.81
IAEA-CO-8	-5.73	-22.37
IAEA-CO-8	-5.67	-22.71
IAEA-CO-8	-5.72	-22.65
IAEA-CO-8	-5.69	-23.07
IAEA-CO-8	-5.73	-22.87
IAEA-CO-8	-5.69	-22.77
IAEA-CO-8	-5.70	-22.27
IAEA-CO-8	-5.71	-22.54
IAEA-CO-8	-5.75	-22.08
IAEA-CO-8	-5.67	-22.72
IAEA-CO-8	-5.63	-22.48
IAEA-CO-8	-5.76	-22.81
IAEA-CO-8	-5.68	-22.83
IAEA-CO-8	-5.67	-22.88
IAEA-CO-8	-5.72	-22.96
IAEA-CO-8	-5.59	-22.55

APPENDIX 2 (Continued)

STANDARD	$\delta^{13}C_{carb}$	$\delta^{18}O_{carb}$
IAEA-CO-8	-5.74	-23.08
IAEA-CO-8	-5.64	-22.89
IAEA-CO-8	-5.64	-22.73

STANDARD	$\delta^{13}C_{carb}$	$\delta^{18}O_{carb}$
IAEA-CO-8	-5.74	-22.68
IAEA-CO-8	-5.67	-22.72
IAEA-CO-8	-5.72	-22.86